Response of Materials Subjected to Magnetic Fields

DARPA DSO grant no. HR0011-08-1-0028

Final Report

Princeton University

Richard Miles. P.I.

August 31, 2011

Report Documentation Page

Form Approved
OMB No. 0704-0188

1. REPORT DATE	2. REPORT TYPE	3. DATES COVERED
31 AUG 2011		**00-00-2011 to 00-00-2011**

4. TITLE AND SUBTITLE	5a. CONTRACT NUMBER
Response Of Materials Subjected To Magnetic Fields	5b. GRANT NUMBER
	5c. PROGRAM ELEMENT NUMBER
6. AUTHOR(S)	5d. PROJECT NUMBER
	5e. TASK NUMBER
	5f. WORK UNIT NUMBER
7. PERFORMING ORGANIZATION NAME(S) AND ADDRESS(ES) **Princeton University,4 New South Building,Princeton,NJ,08544**	8. PERFORMING ORGANIZATION REPORT NUMBER
9. SPONSORING/MONITORING AGENCY NAME(S) AND ADDRESS(ES)	10. SPONSOR/MONITOR'S ACRONYM(S)
	11. SPONSOR/MONITOR'S REPORT NUMBER(S)

12. DISTRIBUTION/AVAILABILITY STATEMENT
Approved for public release; distribution unlimited

13. SUPPLEMENTARY NOTES

14. ABSTRACT

15. SUBJECT TERMS

16. SECURITY CLASSIFICATION OF:			17. LIMITATION OF ABSTRACT	18. NUMBER OF PAGES	19a. NAME OF RESPONSIBLE PERSON
a. REPORT **unclassified**	b. ABSTRACT **unclassified**	c. THIS PAGE **unclassified**	**Same as Report (SAR)**	**25**	

Abstract

This research program examined the interaction of conducting materials with magnetic fields through a series of experiments, the development of analytical models and the development and testing of numerical models. The experiments were a series of drop tests of conducting spheres through strong magnetic field gradients and were used for the development and validation of the analytical and numerical models under low speed conditions. Large decelerations were measured and shown to agree with predictions. These codes were then extended to higher speed conditions and used to examine magnetic compression and the generation of stresses in the high speed materials. Comparisons with the ALEGRA code were made. Scaling models were proposed for high speed interactions where the penetration of the magnetic field into the material is very small during the interaction time. Applications of the magnetic induced stress were explored for changing the impact characteristics of high speed objects against a protective shield, improving survivability.

Introduction

The most significant parameter indicating the effect of a magnetic field on a conducting material is the magnetic Reynolds number, $R_m = \mu\sigma v l$, where μ is the magnetic permittivity, σ is the electrical conductivity, v is the velocity and l is a characteristic scale length. This can be also written as the magnetic diffusion time divided by the interaction time, so for very fast interactions, the magnetic Reynolds number is greater than 1. In this case the induced magnetic field in the material is significant and leads to strong forces opposing the penetration of the external magnetic field into the material. The objective of this project was to examine the effects of conducting materials moving in a magnetic field under conditions where the magnetic Reynolds number is significant. This objective had two foci: 1) To determine if a conducting material moving through a gradient magnetic field at high velocity would significantly slow down, and/or be affected by stresses associated with electrical currents produced by inductive effects. 2) To determine if magnetic flux compression could be utilized to slow down or deflect high velocity conducting materials.

To address the first focus, an analytical approximation was derived for the case of a low velocity (~5 m/s) conducting sphere (~2.54 cm diameter) moving in a gradient (~0.2 m) magnetic field (4 Tesla max), followed by a simulation (modified commercial software) and experiment designed to confirm the approximation. The key result of this was to show that thermal effects were minimal yet the Lorentz forces acting on the sphere were significantly influenced by the radius of the sphere (R^5) and to a lesser extent, the length of the gradient ($1/L^2$) and finally the velocity (v). These forces did slow down the sphere significantly.

The next step was to examine the case of a high velocity (>1000 m/s) conducting sphere. For this case, we used the modified commercial simulation software, verified by the low velocity case. The results showed almost no change in velocity due to the lack of momentum transfer, i.e. too little time in the gradient magnetic field. However, what it did show is that the Lorentz forces were extremely significant. Also, since these forces were asymmetric, the induced stress warped and flattened the

sphere as it traveled in the magnetic field gradient. This was confirmed by Sandia National Laboratory using the ALEGRA code. Thus, while not changing speed, the pressure of impact could be very significantly reduced. A particular application for this was found for the protection of space platforms from space debris. In fact, it was noted that the greatest effect was generated where conventional protection was weakest.

To address the second focus, a well-known analytical approximation of the magnetic flux compression generated by two, 1-D plates (in parallel) moving toward each other (perpendicularly) was verified by the simulation. This was used to show by simulation, in 2-D, how layers could be applied that significantly slowed down an initial mass due to the repulsion force that was produced by the magnetic flux compression. It must be noted that the volume between the plates must be near zero for the effect to be significant. A limitation of this concept had been that if the plates simply folded under pressure and did not collapse completely against each other, the effect would be negligible and therefore not useful for the purpose proposed. This is remedied by using very small plates in conjunction with each other thereby ensuring complete collapse of the volume and generating significant repulsion force. An analytical approximation of the magnetic force produced was developed.

Key Publication: A. Giffin, M. Shneider, and R. B. Miles, "Potential Micrometeoroid and Orbital Debris Protection System Using a Gradient Magnetic Field and Magnetic Flux Compression", *Applied Physics Letters*, **97**, 5, 2010.

Detailed progress and results:

Results of this program can be broken into four areas:

1) Experimental tests conducted in high magnetic fields for the development of benchmark measurements for validation of both analytical and computational models.

2) Development of analytical models for comparison with computational results for conditions that cannot be duplicated in the laboratory

3) Implementation of 3-D commercial code for modeling of dynamic interactions in conducting materials moving though high magnetic fields.

4) Primary analysis of effects on a conducting sphere moving at high velocity with use of modified 3-D commercial code.

5) Results using the ALEGRA code for the high velocity conducting sphere including deformation.

6) Primary analysis of effects of multiple plates utilizing magnetic flux compression.

7) Possible application implementing results and current technologies.

8) Additional analysis of various models in literature and off shoots of current ideas.

9) Current and future directions

Areas 1) and 2) Experiments and Analytical Model Development

Figure 1 shows the laboratory set up for the benchmark experiments. The magnet is a superconducting Helmholtz coil capable of operating at up to 6 Tesla. Access to the high magnetic field at the center of the magnet is by three orthogonal passages, including a vertical passage through which spheres are dropped and a horizontal passage through which a laser beam is passed for timing the arrival of the spheres at the center. For the experiment, various solid, hollow or thin shell metallic spheres were dropped into the magnetic field and the fall time from release to the arrival at the center of the field is recorded using laser beams, as shown diagrammatically in the pictures. The interaction of the magnetic field with these spherical objects leads to the development of eddy currents that produce an induced magnetic field that generates a force opposing the gravitational force, thus reducing the fall velocity and increasing the fall time.

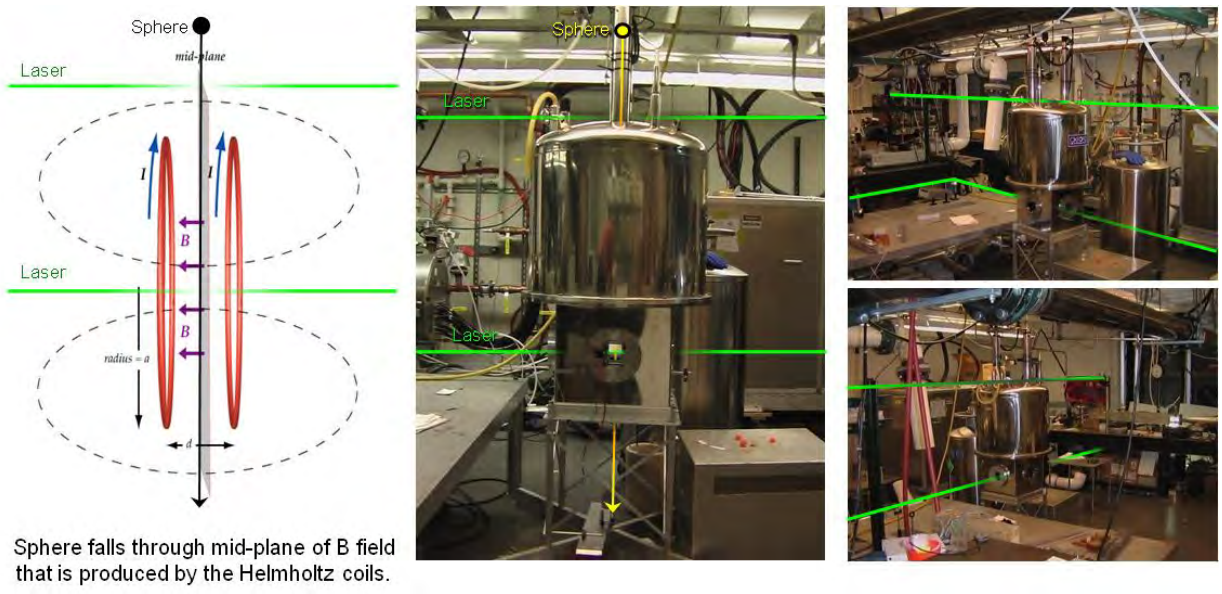

Figure 1: Geometry of the Helmholtz magnetic coils and photographs of the laboratory set up. Spheres are dropped through a vertical hole (yellow line shows the fall trajectory) and pass into the high field region at the center of the magnet coils. The fall time is recorded by a pair of laser beams as shown in green.

Figure 2 shows the induced force on a falling solid sphere. The force is produced by the induced eddy currents. As the sphere moves through the external B field ($\mathbf{B}_{ext}$) that is static but increasing along the x-direction, a current ($\mathbf{I}_{ind}$) is induced in the z,x-plane (the **E** field). The view of the left plane is rotated on the right side so that the external B field is coming out of the plane while the induced B field ($\mathbf{B}_{ind}$) is directed into the plane. In both cases notice that the direction of the force is radially inward, with a net force opposing the motion. As the velocity increases, the induced currents become more confined to the outer perimeter of the sphere, and at high velocity the forces that are generated in a thin shell sphere and the forces generated in a solid sphere at equal velocity are almost identical.

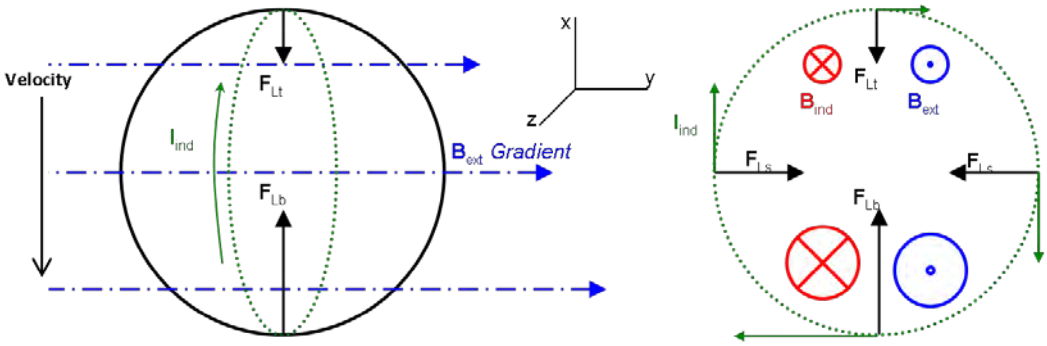

Figure 2: Induced current and induced forces associated with a sphere dropping through a positive magnetic field gradient. The left diagram is a view of the sphere seen from a position orthogonal to the magnetic field lines and the right diagram shows a cross section of the sphere seen from a position along the magnetic field lines. The directions of the induced currents and force vectors are indicated.

Figure 3 shows the analytical model approximation. The actual magnetic field reverses sign as shown by the red curve on the right diagram. The analytical model uses a piecewise linear approximation shown in blue. The most important feature of the field is the gradient and the linear approximation accurately captures that slope. The relevant quantity is B_{max}/L, the maximum magnetic field divided by the liner dimension over which that field changes from 0 to the maximum value.

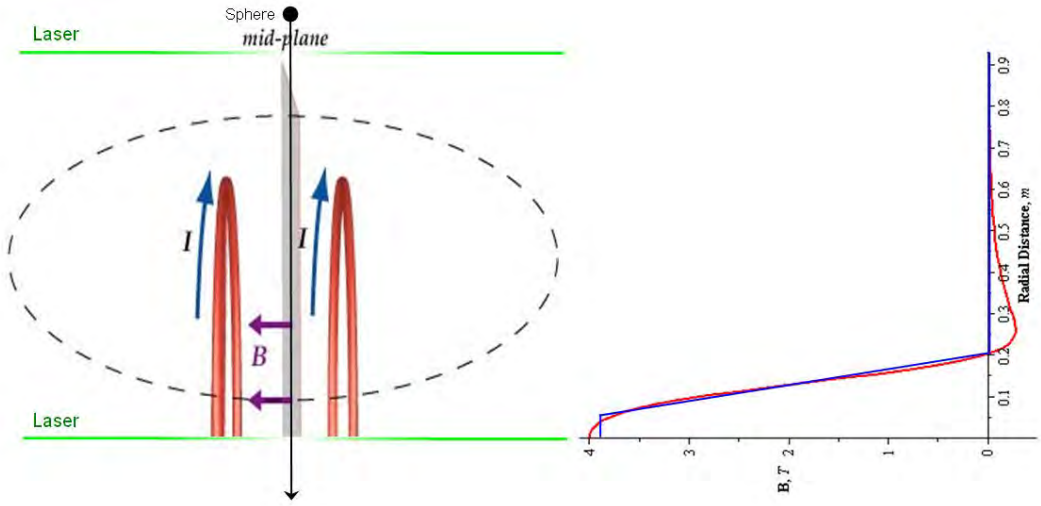

Figure 3: Modeled and actual magnetic field gradient. The actual gradient is calculated from the specifications given for the magnet. The modeled field is a piecewise linear approximation.

Figure 4 shows the results of the drop tests and the analytical predictions. Both aluminum and copper alloy spheres were tested. The ½ " diameter (6.35 mm radius) copper sphere had a conductivity that was 93% of the International Annealed Copper Standard (IACS) and had a fall time that was very close to the predicted time and close to the ideal copper fall time. As the formula above the figure indicates, the force that is generated is proportional to the product of conductivity, σ, and the velocity, *v*, times the 5th power of the sphere radius, so the ¾" and 1" diameter (9.52 mm and 12.7 mm radius) aluminum spheres are much more strongly affected. The aluminum alloy in those spheres is less conducting than the ideal aluminum alloy, which has 60% the conductivity of pure copper. In these cases the conductivity was only 32% and 38% of IACS for the ¾" and 1" aluminum spheres. The significant difference in the fall times associated with the same size aluminum and copper spheres is because of the different density of the two objects: the aluminum alloys are much lighter than copper. Note that the fall time for the solid 1" aluminum sphere is almost three times that of free fall. The analytical model captures the fall times to within 4% of the measured value.

These experiments have allowed for the development and testing of an analytical model that forms the foundation for the validation of computational results. The falling spheres are large enough and move fast enough under gravitational acceleration to produce significant magnetic Reynolds number effects. The close agreement of the analytical model with the measured results indicates that the model is

capturing those effects accurately and thus can be expected to be reliable for higher velocity and more complex high magnetic Reynolds number simulations.

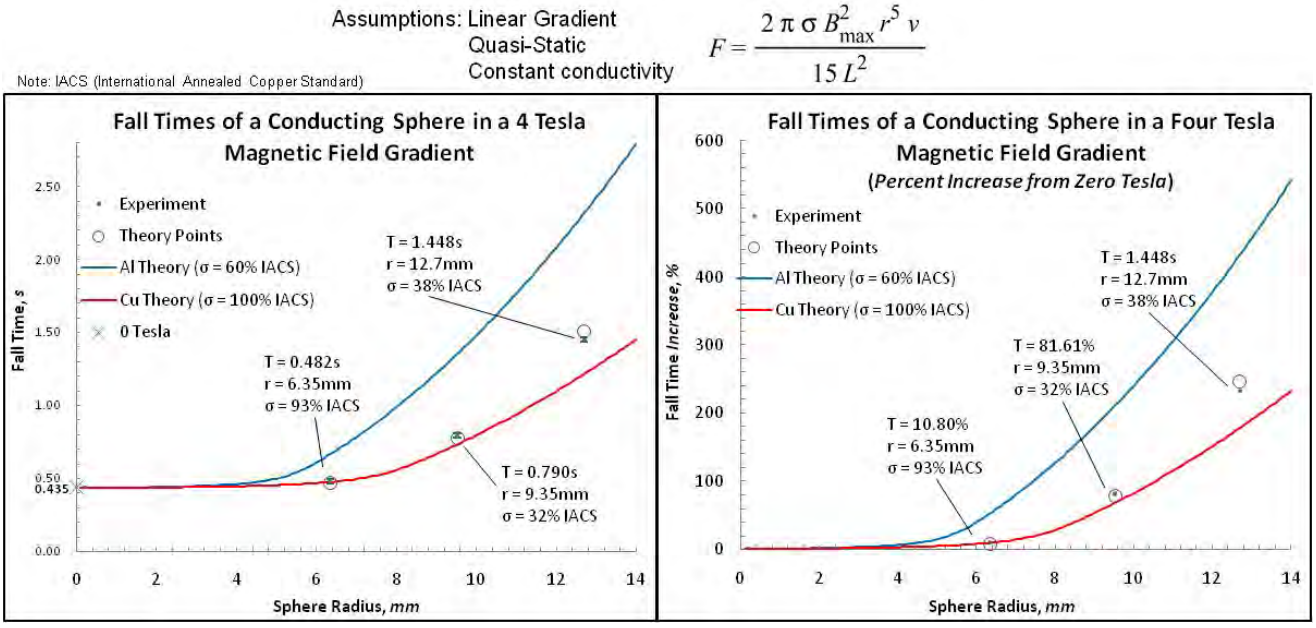

Figure 4: Results for drop tests of ½" diameter copper and ¾" and 1" diameter aluminum solid spheres. The left hand diagram shows the recorded and predicted fall times. The right hand diagram shows the recorded and predicted percentage increase in fall times. Note that the aluminum alloys had conductivities that were significantly lower that the ideal conductivity of aluminum which is 60% of the International Annealed Copper Standard (IACS).

Area 3) Modified Commercial Software

In order to provide for further validation of the code that is under development, we purchased a versatile commercial software package, MagNet by Infolytica Corporation. Following an extended series of demonstration tests conducted by the company in order to determine the utility of the code for our purposes, the first component of the software was acquired on 10/27/08. This software uses finite element analysis to simulate electromagnetic effects on materials. The code can simulate dynamic interactions of metals with magnetic fields, but it does not have the capability of following any deformation of the metal objects and needs to have material properties specified before the run. The code is very useful for simulating high Reynolds number effects, magnetic field compression and forces on objects. It has a full 3-D capability. Training for use of the software was completed on 11/21/08.

Figure 5 shows the comparison between the analytical approximation and the simulated model results using our modified 3-D software. Comparing these results further validates our computational software. This increases our confidence that the simulated results at high velocities (high magnetic Reynolds numbers) are accurate for real situations. Further, it also validates our analytical approximation that shows the force as $F \sim \sigma G^2 v r^5$ where σ is the conductivity, v is the velocity, r is the

radius of the sphere and the field gradient, $G=B_{max}/L$ is the maximum magnetic field, B_{max} divided by the length, L of the gradient.

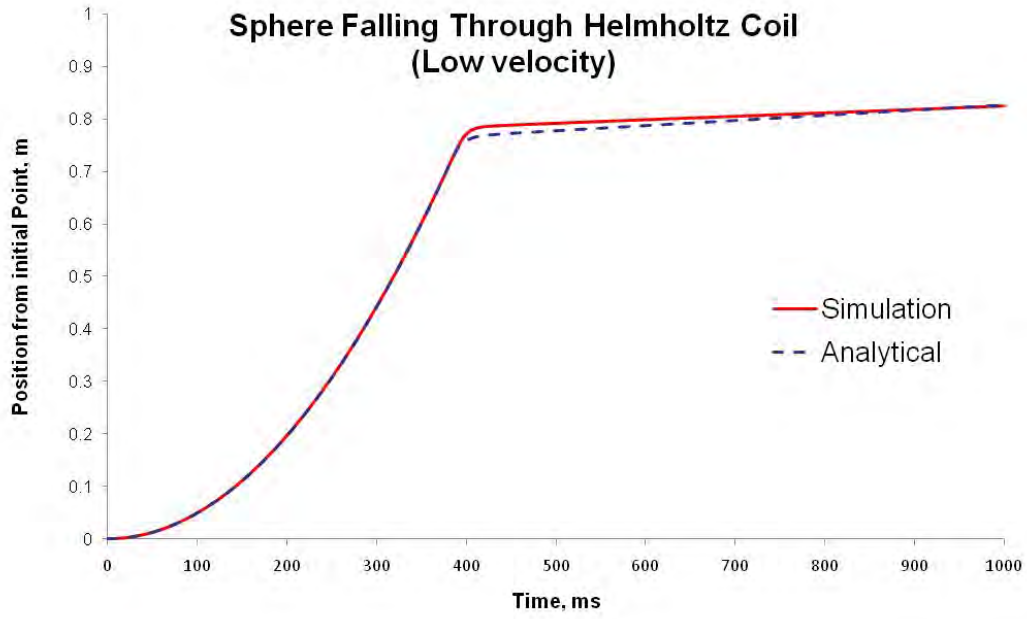

Figure 5: Comparison of analytical approximation and simulated numerical results using modified commercial code.

Figure 6 shows the acceleration and velocity changes in a sphere moving at low velocity (as above). Notice that the acceleration changes sharply at around 450 msec. At this time the sphere enters the first significant change in the field; the beginning of the field gradient. It almost instantly reaches a terminal velocity at this point as can be seen in the second graph. The sphere stays at this velocity until it reaches the end of the gradient. As can also been seen, toward the end, the sphere begins to increase in speed again. This is due to the fact that the gradient is not linear and tapers off at the end. We will not concern ourselves with this as our primary focus is the initial change.

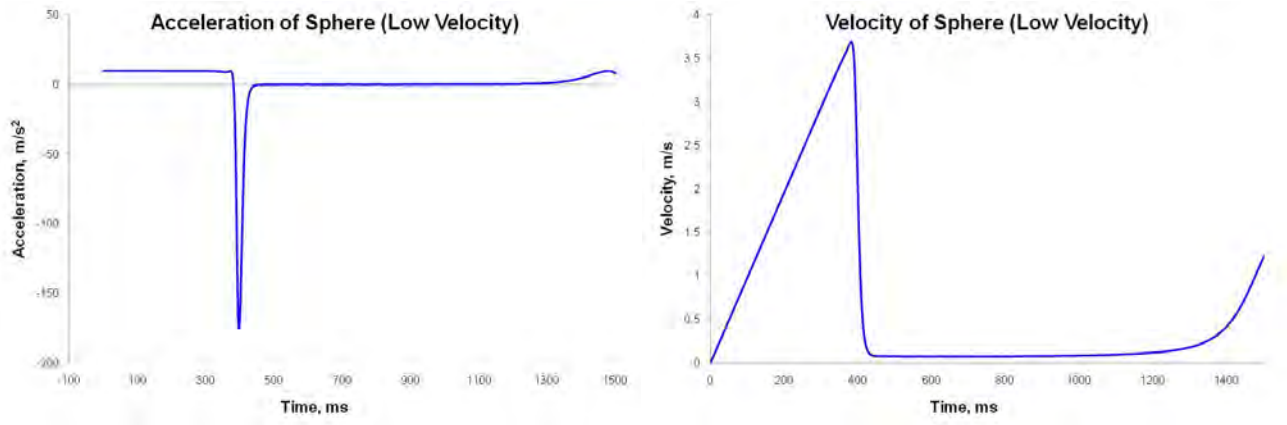

Figure 6 These two graphs show the changes in the acceleration and velocity as a conducting sphere moves through the magnetic field gradient (0 to 4 Tesla over ~20cm) at low velocity (under the influence of gravity for 1 meter).

Area 4) High Velocity Conducting Sphere

Figure 7 shows the deceleration of a copper sphere of the same size and magnetic field as above, but it is traveling at high velocity (1 km/s). Notice the much larger deceleration, about 50 times greater than the low velocity case. However, in this case the reduction in velocity is minimal over the distance of the gradient (less than 1 m/s), even though there is a large deceleration as shown. This is due to low momentum exchange over the time of the travel.

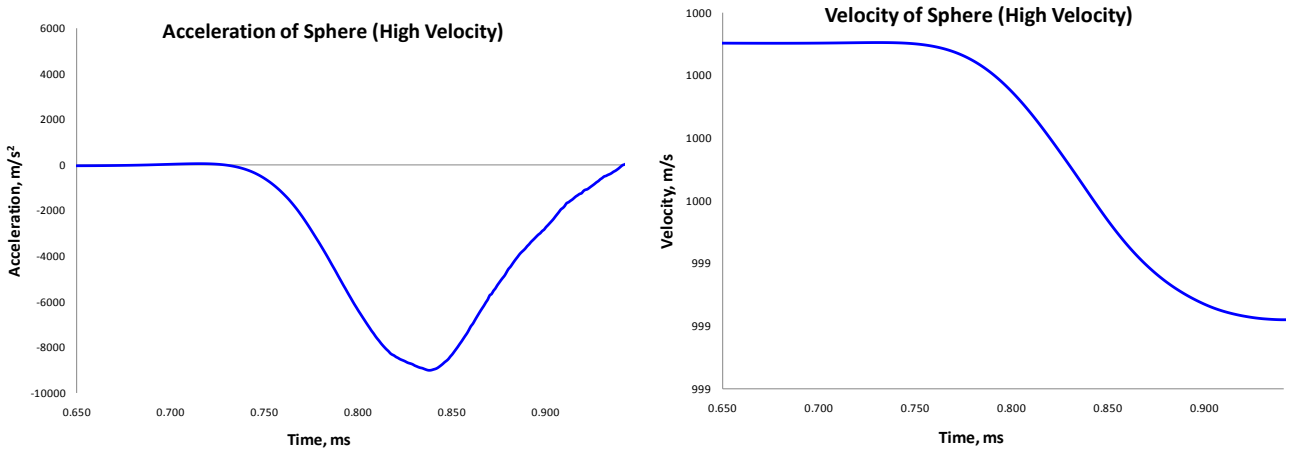

Figure 7 These two graphs show the changes in the acceleration and velocity as a conducting sphere moves through the magnetic field gradient (0 to 4 Tesla over ~20cm) at high velocity (under the influence of gravity for 1 meter).

Figure 8 shows a 3-D surface picture of the induced force on a falling solid copper sphere with a radius of 12.7 mm (1" diameter) at 1 km/s, putting it into the high Reynolds number regime. The magnetic field goes from 0 T to 4 T over a span of ~20 cm in the x direction. As the sphere travels through the gradient, the color and arrows indicate the strength (red = strongest) and direction (approximately radial) of the pressure on the sphere. The largest forces are at the bottom of the sphere which has the effect of slowing down the sphere. At high velocities, this reduction in velocity is minimal over the distance of the gradient, again due to low momentum exchange. However, the forces become very large as the velocity or gradient increases due to the increased strength of the eddy currents. Therefore, the key aspect to note is the *differential* of the forces acting on the sphere. These forces will flatten and extrude the sphere into a scalene ellipsoid shape. Thus the pressure of the impact of the sphere against another object will be diminished.

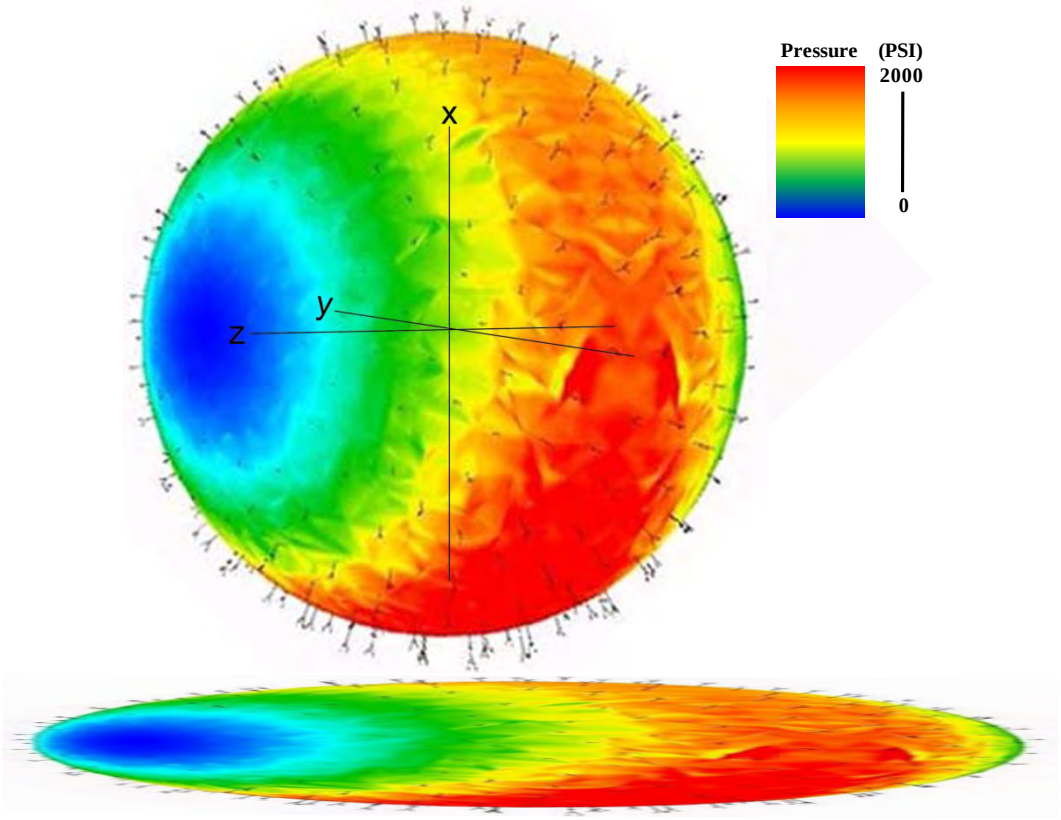

Figure 8: The top picture is a 3-D surface picture of a sphere moving through a magnetic field gradient. As the sphere travels through the gradient, the color and arrows indicate the strength (z = 0 plane is strongest, z axis is weakest) and direction (~radial) of the pressure on the sphere. The bottom picture is a 3-D representation of the sphere above as forces flatten and extrude the sphere into a scalene ellipsoid shape.

An analytical formulation of the force is very difficult to derive since the high velocity regime is characterized by non-linear currents and a highly perturbed magnetic field. However, we can still make a qualitative estimation, if not a roughly quantitative approximation for the force under these conditions using the low velocity equation. In this case, we can assume that the current is mostly confined in the skin layer of the sphere. Therefore, if we calculate the force that is due to the shell of the sphere that has a thickness of the skin layer, we should see reasonable results which are shown in table 1.

Table 1

Mag Reynold's #	Simulation, m/s^2	Approximation, m/s^2	Percent Error
350 (1000 m/s)	12444	14060	13.0%
920 (2631 m/s)	15400	23338	51.5%
1750 (5000 m/s)	16325	32585	99.6%

As can be easily seen, the change in the magnetic Reynolds number is almost directly equivalent to change in the percent error. We can adjust for this with an appropriate adjustment to the skin

depth, $\delta = \frac{r}{\sqrt{R_m}} \frac{e^{-.0004 \cdot R_m}}{\sqrt{\pi}}$, where the left fraction is the diffusion depth definition rewritten using the Reynolds number and the right fraction is our empirical adjustment. Note: Classically the skin depth is equal to $\sqrt{2/\mu\sigma\omega}$ where ω is the angular frequency of the signal. However, this is for the special case of a sinusoidal signal.

For an analytical solution, the correct magnetic field in the sphere is needed. Since full solutions to this problem can only be arrived at numerically, analytical approximations are sought. To this end, typically an exponentially changing magnetic source is used (skin layer method). This only applies to the surface of the conducting object due to the compression of the field there. However, from the reference frame of the sphere in our case, we not only have this exponential source, but it is changing due to the gradient as well. Therefore, the approximation that we need for the high velocity case must contain both sources. A solution was found for diffusion due to a steady state, sinusoidal changing source. We can manipulate a sign wave to approximately mimic the field that is produced by the Helmholtz coil field as seen in figure 9.

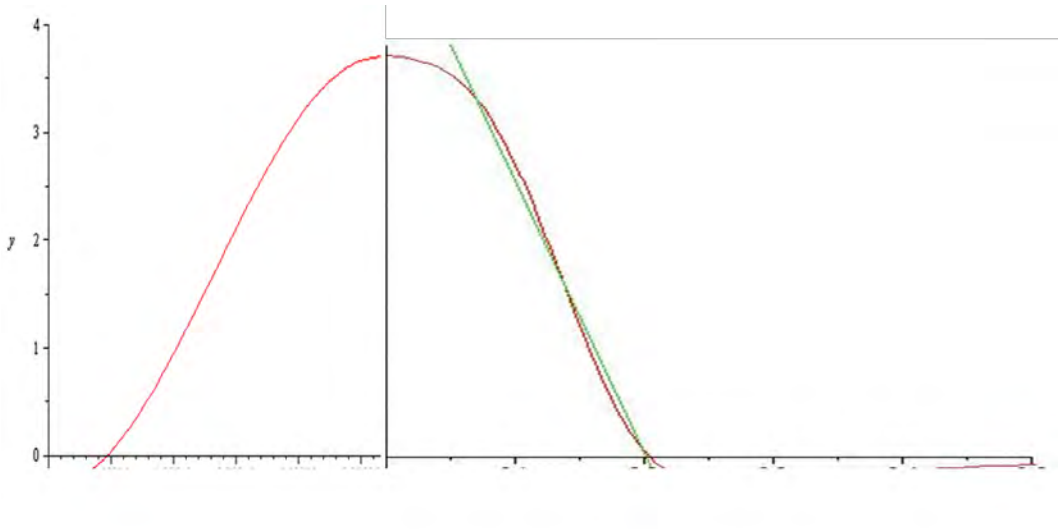

Figure 9: On the left is a portion of a sinusoidal signal which mirrors the Helmholtz configuration on the right.

The resulting field equation inside the sphere along its axis would be,

$$H(x) = H_0 e^{\frac{t}{\tau} - \frac{x}{\delta}} \left(\frac{1}{2} cos\left(\frac{\pi \cdot t}{\tau} - \pi - \frac{x}{\delta} \right) + \frac{1}{2} - 0.075 \right)$$

Figure 10 shows the comparison between the resulting solution and the simulation.

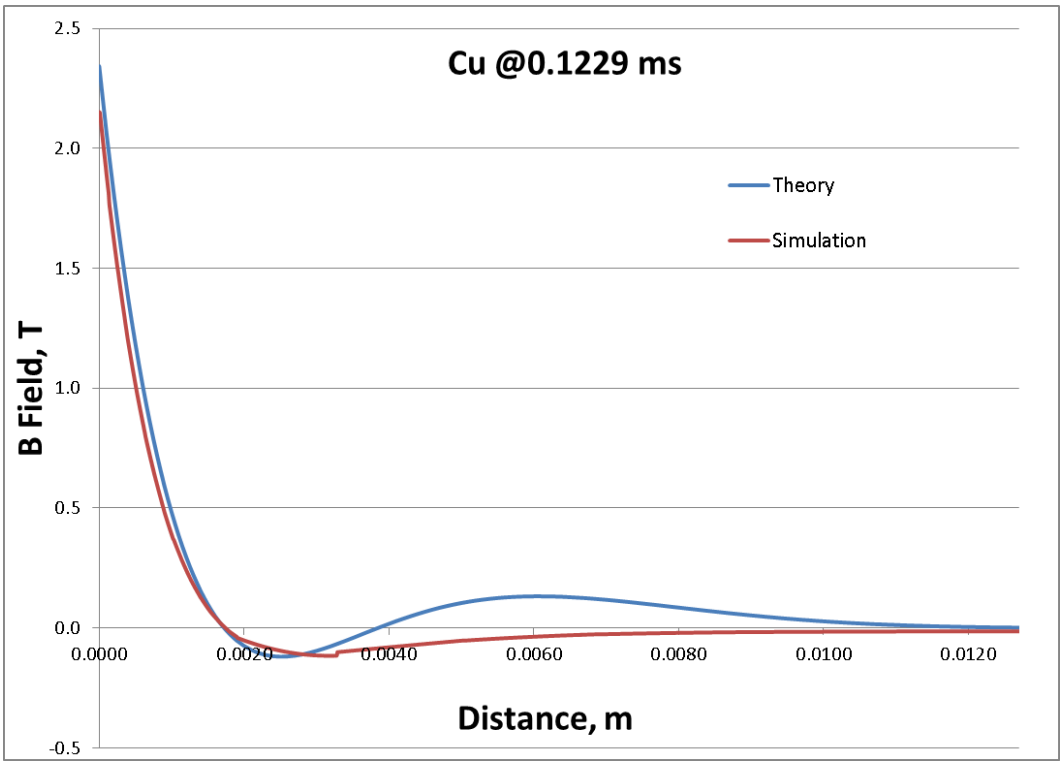

Figure 10: Comparison between the approximate solution and the simulation.

While the source signal is close, the plot shows how even a small difference in the slope of the magnetic field gives rise to clear changes.

Area 5) Results using the ALEGRA code.

Figure 11 shows simulations run with the ALEGRA code versus our modified commercial code. Again, a conducting sphere is moving through the magnetic field gradient (0 to 4 Tesla over ~20 cm) at high velocity (under the influence of gravity for ~1 meter). The red curve was run with a very course mesh. The green was run with a finer mesh. This comparison clearly demonstrates that the ALEGRA solution is converging with our modified commercial code. This gives us confidence to use the ALEGRA code to study the effects of deformation of the sphere.

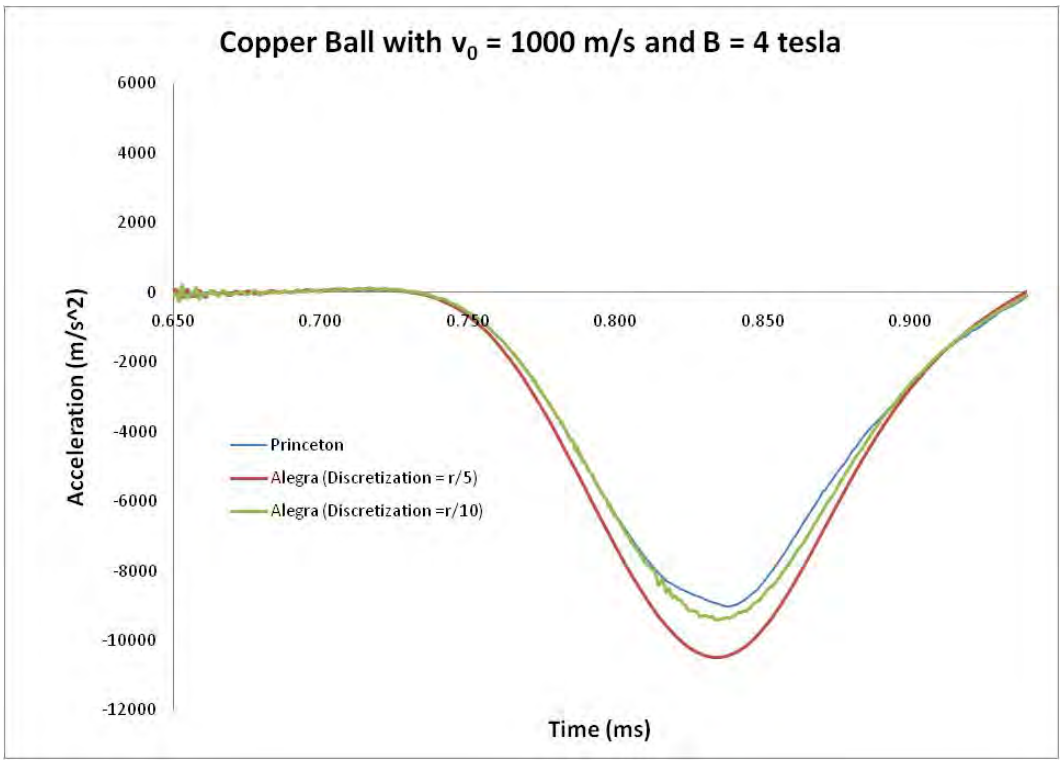

Figure 11: This graph compares the solutions of the modified commercial code (blue) and the ALEGRA code. The red curve was run with a very course mesh. The green was run with a finer mesh. This shows that the ALEGRA solution is converging with our modified commercial code.

Figure 12 shows simulations run with the ALEGRA code at various velocities of a solid copper sphere moving in a gradient with length ~ 20 cm and a maximum field of 40 T, and the associated maximum *plastic* deformation. Note that plastic deformation is irreversible deformation. At all velocities where the maximum field is 4 T, very little plastic deformation is observed. It should be noted that if the gradient length were smaller, this effect would increase. To help illustrate the deformation effect, we have only included a 40 T case. Notice that regardless, the deformation peaks at 3 km/s. Lower than 3 km/s, the forces are smaller. Above 3 km/s, the sphere has less time for its momentum to change, although it experiences larger forces.

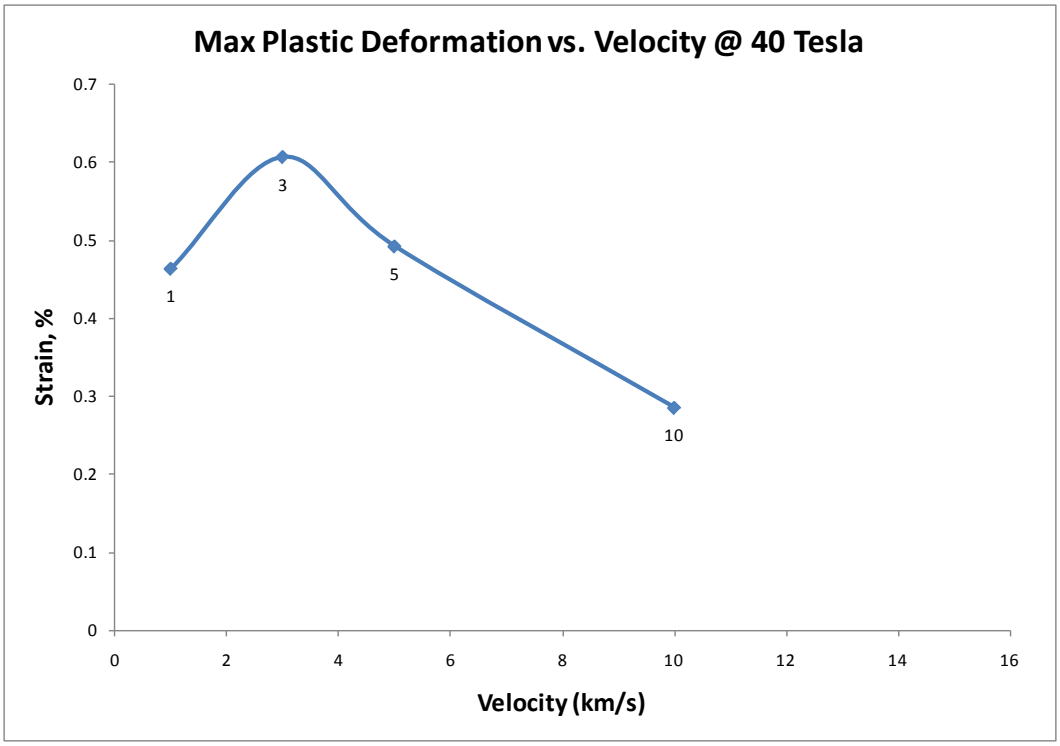

Figure 12: The graph shows the maximum plastic strain for a solid copper sphere at various velocities in a gradient with length ~ 20 cm and a maximum field of 40 T with solutions generated using the ALEGRA code.

The solutions for the above cases took between 1 – 3 hours to run on a bank of 64 processors. Although they are adequate for this illustration, to compare with our modified commercial code the solutions require a much longer run time. This time varies but is comparable to our modified code run times, ~ 30 hours. The difference is that our code currently runs on one processor. Also the ALEGRA code can take anywhere from 0 to 48 hours to even begin since it must wait in a queue. Therefore, although our code does not include deformation, one can see the benefits of using it for preliminary confirmation and analysis of the physics, determining initial conditions as well as comparative analysis between codes.

Area 6) High velocity conducting plates

Next we simulated two semi-infinite copper plates with constant conductivity moving toward each other in a magnetic field at constant velocity. The simulation was compared with the theoretical solution for this case presented in "Compression of Magnetic Field between Two Semi-Infinite Slabs of constant Conductivity" by Paton and Millar[1]. Important parameters in the effective utilization of the code are the grid geometry and scale, and this exercise provided a quantitative way to explore those sensitivities. It was found that the computed solution converged toward theoretical prediction as the grid was refined, and that provided confidence in the both the accuracy of the code and in the accuracy of the analytical models.

Studies of the two plate configuration were then followed by a three plate dynamic simulation showing the compression effects with one plate suspended between an upper plate and a fixed lower plate. This simulation assumed an initial velocity and momentum of the upper plate, but then let the momentum and induced forces control the changes in velocity and position of the upper and middle plates. The geometry selected for all three plates has thin 1 mm thick copper surfaces covering 1 cm thick non-conducting slabs. The upper and middle plates are separated by 5 cm from each other and the middle plate is separated by 5 cm from the bottom. The initial 2-D geometry is shown in figure 13. The 5 Tesla magnetic fields produced in the two gaps are formed by high temperature superconducting layers that are placed between the 1 mm copper layer coverings and the non-conducting dielectric slabs and forming two solenoids. The first solenoid surrounds the upper gap and the second surrounds the lower gap. The current loop in these solenoids is completed using the 2-D capability of the model, but the diagrams shown here are a 1-D representation of the cross section. The location of the 1mm copper layers suppresses magnetic quenching of the superconductors during compression since the current surge is taken by the copper and the superconductor does not see the large magnetic field increase.

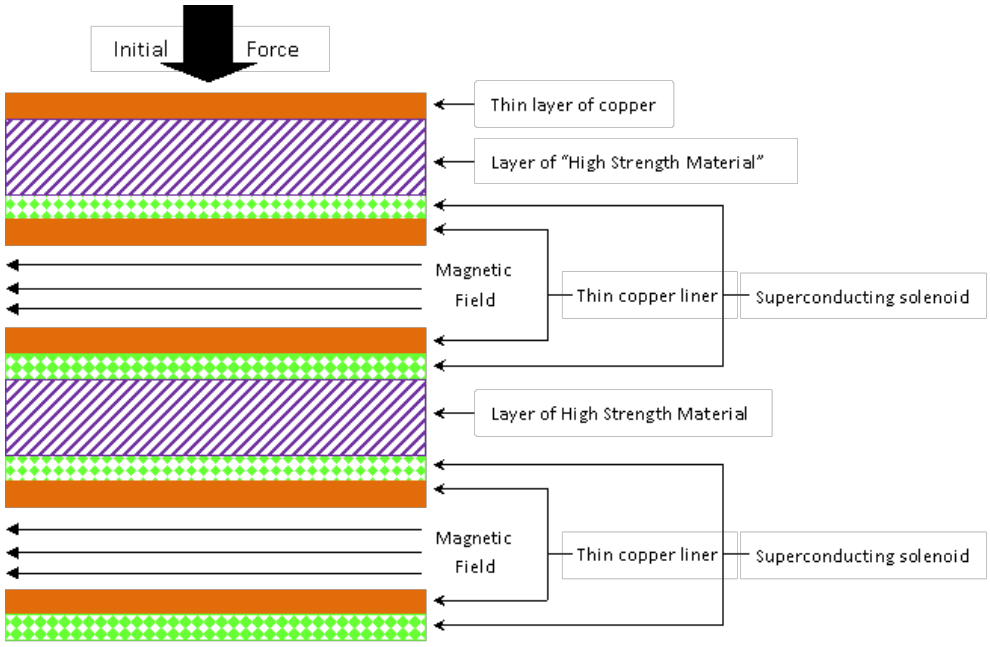

Figure 13: Three layer configuration with copper coated dielectric materials and thin superconducting material for generation of the initial magnetic field in the two gaps separating the three plates.

A uniform force is initially placed on the upper plate causing it to move at 1000 m/sec and to compress the magnetic field in the upper gap. This compression, in turn, leads to a force on the middle plate. The momentum of the top plate is transferred to the middle plate without contacting it, and the middle plate is accelerated down toward the stationary lower plate. As the magnetic field in the lower gap between these two plates compresses, the middle plate slows, reverses direction, oscillates, and then rebounds, transferring its momentum back to the top plate and accelerating it upward.

An animation of the simulation using the above configuration have been made using MagNet. Figure 14 shows this oscillatory motion of the middle plate as a function of time in composite images, and

figure 15 shows the force felt by that plate, indicating an initial peak associated with the compression of the magnetic field in the upper gap by the upper plate moving toward the middle plate, a subsequent compression of the field between the middle and lower plates and then force reversals leading to the oscillations. Note that the peak force occurs when the middle plate approaches the bottom plate. The conductivity in the copper layers acts to dissipate the energy associated with the initial motion of the upper plate, so the rebound is not at the full initial velocity. The model does not yet properly include reduced conductivity associated with material heating, but the dissipation produced even with this approximation is 80% of the initial energy of the moving top plate.

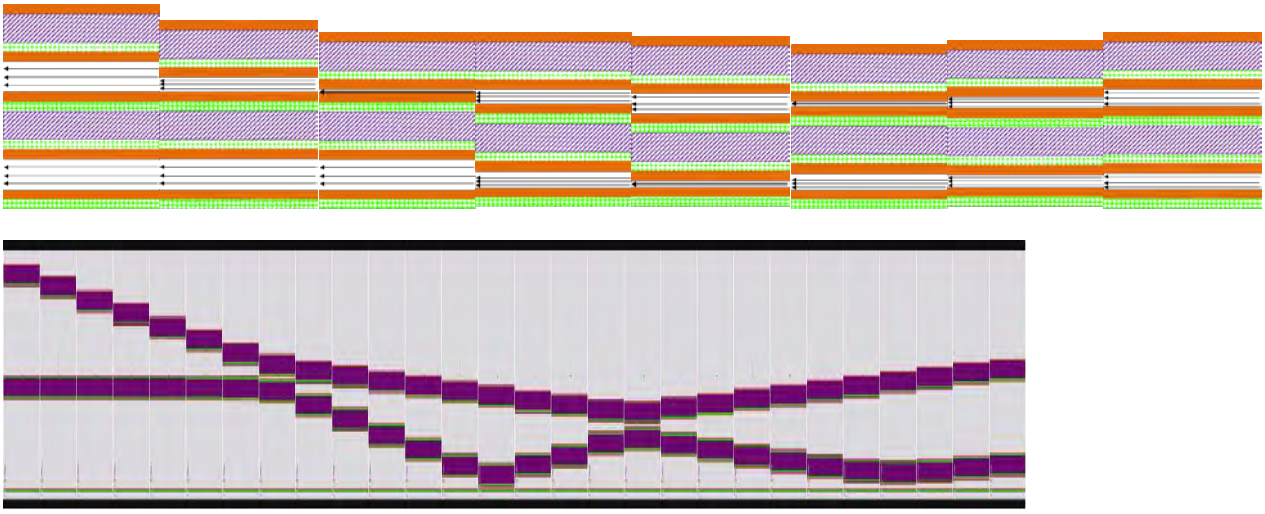

Figure 14: Displacement of the plates a various time steps during the compression showing oscillation of the middle plate and subsequent repulsion of theupper plate.Upper figure shows 28 sequential times steps The lower figure shows a longer sequence with more time steps highlighting the oscillation of the middle plate.

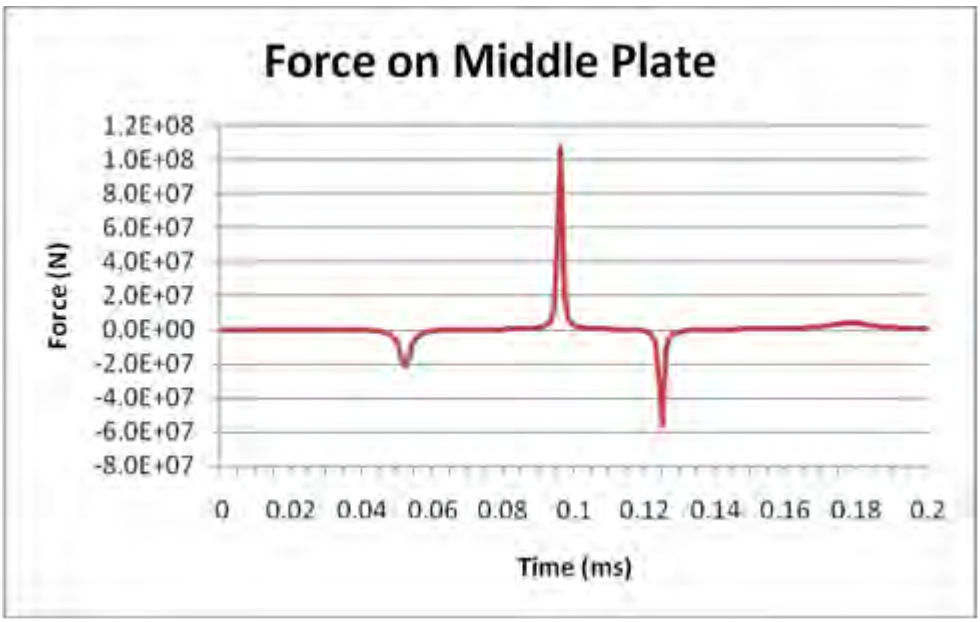

Figure 15: Force felt on the middle plate as a function of time.

Area 7) Possible Application Implementing Results

Events such as the Chinese ASAT test in January 2007 and the Iridium-Cosmos collision just over two years later have brought the problem of orbital debris into sharp focus. The RAND Corporation stated that orbital debris "is the gravest threat to new and existing space systems." An example of current shielding for micrometeoroid and orbital debris (MMOD) is on the International Space Station (ISS) which uses a "bumper" and "catcher" setup[2]. The intent is for the object to hit the "bumper" (aluminum) at high velocity and melt due to the impact, then spread out (due to material design) across the "catcher", thus distributing the force over a greater area.

Figure 16 shows a possible application for our research as protection against space debris. Although, most debris is non-metallic, the current configuration of the International Space Station (ISS) shielding uses a "bumper" and "catcher" setup as shown. The idea is that the debris will hit the "bumper" (aluminum), melting due to impact and spread out (due to design) across the "catcher", thus distributing the force over a greater area. Since, as previously stated, in the high magnetic Reynolds regime the currents are produced in the outer surface (skin), the effect of the magnetic field would be concentrated on the aluminum. This would cause the aluminum to spread out and induce a large force on the incoming debris so that it spreads out as well. Therefore, if this system also included a magnetic field as shown, the forces on the mass could potentially be further spread out and slowed. This may result in the need for less shielding. Additionally, the current protection configuration is weakest when the debris is larger than 1" or is not moving fast enough to melt on impact. Our implementation could also help in this regard for metallic objects. The force is proportional to radius, R^5 so the bigger the object, the greater the effect. Also, the slower the debris was coming in, the more time would exist for

deformation. We suggest that this is feasible using currently produced high temperature superconducting materials.

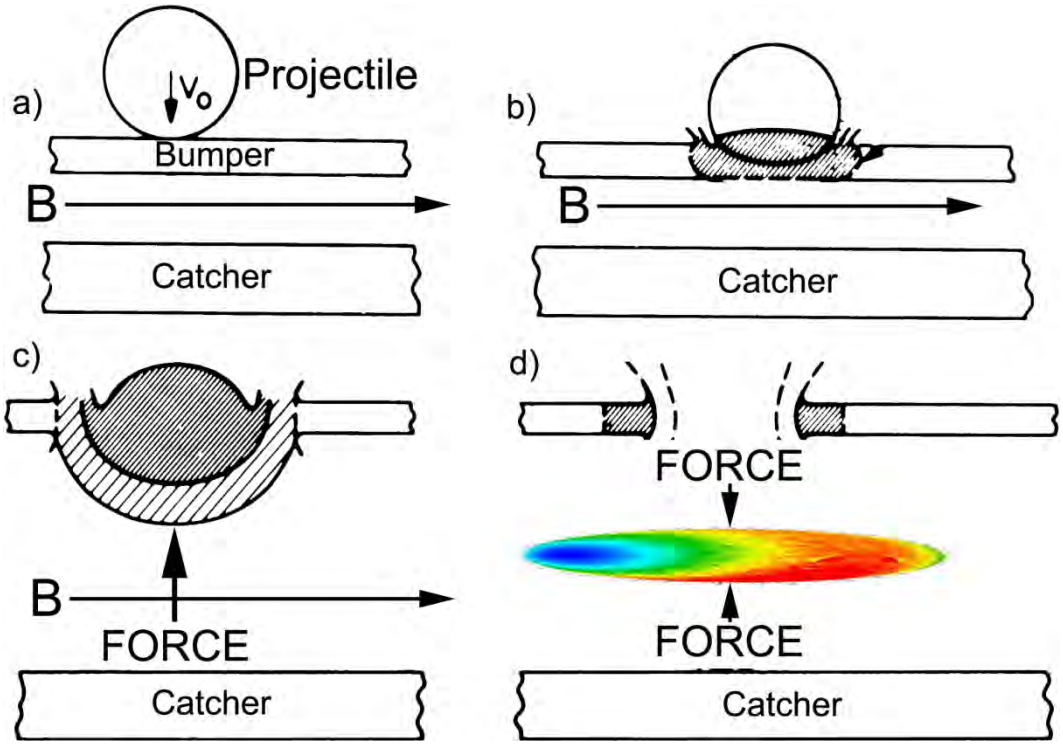

Figure 16: As the object hits the "bumper" it traverses a magnetic field gradient inducing forces that deform and slow the mass.

Figure 17 shows a graphic of information accumulated from ISS shield testing[2]. The area above the curve represents failure of the shielding for various projectile sizes and various impact velocities on the current shielding configuration. As mentioned above, the shielding is particular weak around the 3 km/s range. If one superimposes figure 12 onto figure 17, one can see that at the velocity where the current shielding is the weakest, the deformation of the sphere in our simulations is the strongest, see figure 18. Thus it seems that our configuration could compliment the current shielding. Further, as noted above, the force is proportional to radius, R^5 so the bigger the object, the greater the effect.

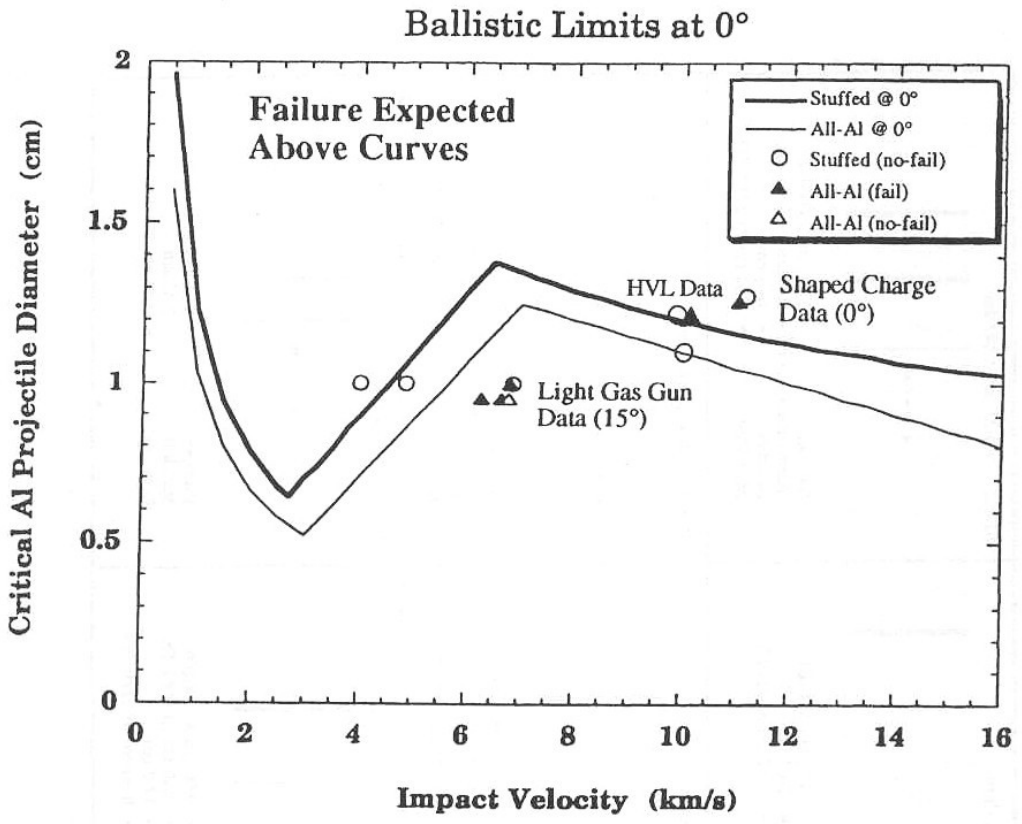

Figure 17: Above is a graph displaying information accumulated from ISS shield testing[2]. The area above the curve represents failure of the shielding for various projectile sizes and impact velocities on the current shielding configuration.

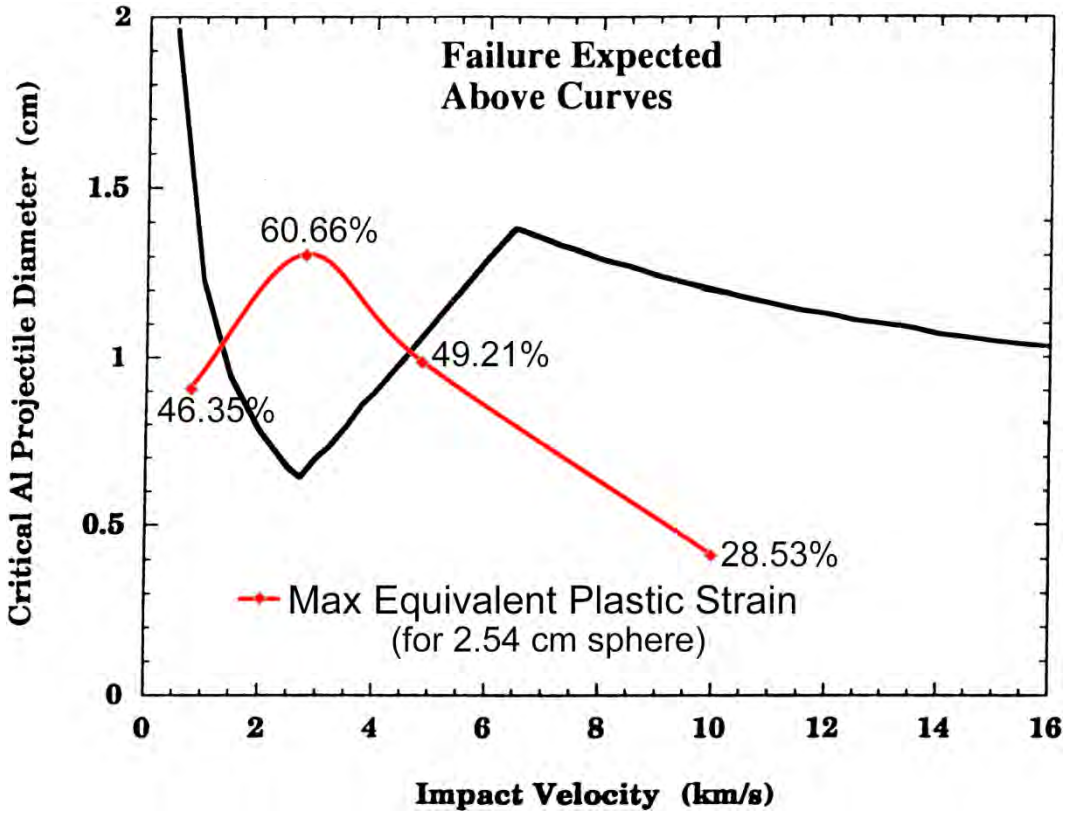

Figure 18: Greatest deformation due to the magnetic field gradient (top curve) tends to occur when the conventional protection is weakest.

The effect of the magnetic shielding can be increased significantly if magnetic flux compression occurs. When a magnetic field is surrounded by a conducting material, the field diffuses through the material at a certain rate producing eddy currents. These currents then produce an induced field inside the material that effectively cancels the now time varying field (the skin effect) as it attempts to diffuse out of the cell. If the conductor shell collapses faster than the field can diffuse out (high Reynolds number regime) the field becomes "trapped" by the conductor. As the conducting shell continues to collapse around the field, the magnetic flux is "compressed" which results in an increase in the magnetic field. This is a well-known technique for creating very large magnetic fields for brief periods of time. Of course this means that the magnetic pressure is increased as well, $P_m = B^2/2$. We can take advantage of this effect by using a very thin walled simple cubic lattice made out of a conducting material for shielding. The walls are made thin because the skin depth will be very small in the high Reynolds number regime. This also helps in reducing the weight. In the rapid collapse limit, when the cells of the lattice are fully collapsed, the resulting magnetic field will be scaled according to $B \sim B_0 R_m$ where B_0 is the initial field and the characteristic length in the magnetic Reynolds number is the length of the gap between conductors. Therefore the pressure induced can increase to, $P_m \sim (B_0 R_m)^2/2$

To achieve this, the cells inside need to be small to ensure that they become fully collapsed since the effect is not significant otherwise. Obviously if the cells in the lattice are very small, the gap will be very small, reducing the magnetic Reynolds number. However, since the conducting cells are all connected, the gap for the magnetic Reynolds number is effectively the sum of all the lattice cell gaps

(the pressure is additive). This concept is visualized with a simple cubic conducting lattice in a uniform magnetic field in figure 19.

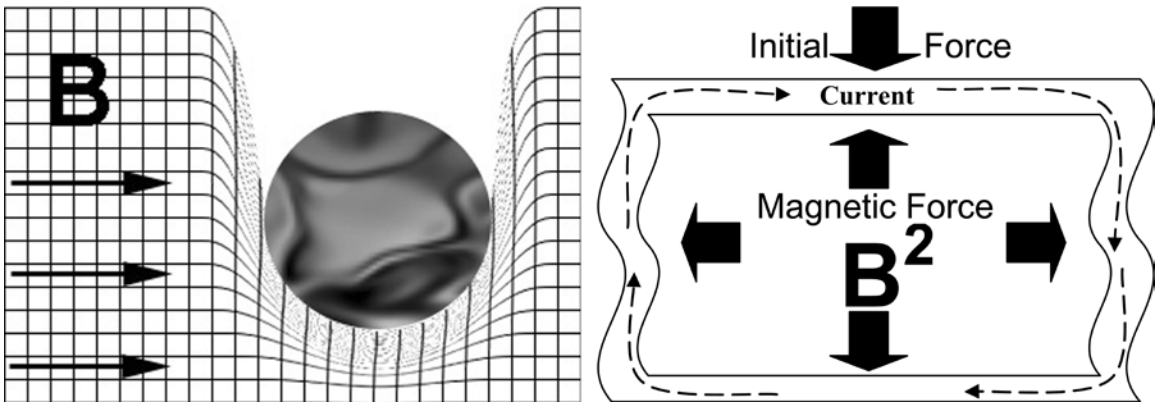

***Figure** 19: Left - As a projectile crushes the lattice, the uniform magnetic flux in each cell is compressed which dramatically increases the magnetic field inside to, $B \sim B_0 R_m$. Right - When a cell is compressed, the magnetic field exerts a pressure proportional to $P_m \sim (B_0 R_m)^2/2$.*

The exact magnetic field inside the collapsing cell is difficult to obtain. As an approximation, we use the skin layer method to determine the field strength. Cylindrical geometries for experimental flux compression have been used in the past. These geometries allow a very simple approximation. However, with a two sided box, the approximations are more difficult simply because more assumptions need to be made. Depending on the assumptions, the Magnetic field that would be produced is $B = B_0 \left(\frac{l_0}{l}\right)^{1-\frac{\alpha}{R_m}}$ where l_0 is the initial length, R_m is the magnetic Reynolds number and $1 \leq \alpha \leq 2$ depending on the approximation used.

The two concepts discussed above can be used separately or together depending on the application. To combine them, a uniform magnetic field can be generated for the lattice. Then as a projectile begins to crush the lattice, the projectile velocity and energy will be reduced. If the lattice is pierced, the object will suddenly enter a gradient in each lattice cell. Thus the projectile will be effectively entering a sequence of very short gradient fields. This is a benefit as the force is inversely proportional to the gradient length squared.

Area 8) Additional Analysis of Various Models.

Figure 20 shows the forces inside a cylinder as opposed to a sphere. The direction of the magnetic field is pointing out of the page. As the cylinder travels through the gradient, the color and arrows indicate the strength (red = strongest) and direction of the force on the cylinder. The purpose of this model was twofold: 1) to model different geometries. Notice that the force (which is a reflection of the current) has a non-spherical shape and sharp corner effects. These corner effects contribute to a large increase in computational power needed. 2) To show that the object would rotate in the field if initially asymmetric. The orientation of the cylinder on the left is set so that the object initially falls down in a symmetric way. Because of the symmetry, the forces are balanced against each other and the cylinder is in a stable equilibrium. Thus in the absence of perturbations, the cylinder will not rotate. The

orientation of the cylinder on the right shows that the cylinder is initially offset from the normal axis. As it moves down, there is a noticeable asymmetry in the force. This asymmetry will cause the cylinder to be unstable and therefore rotate.

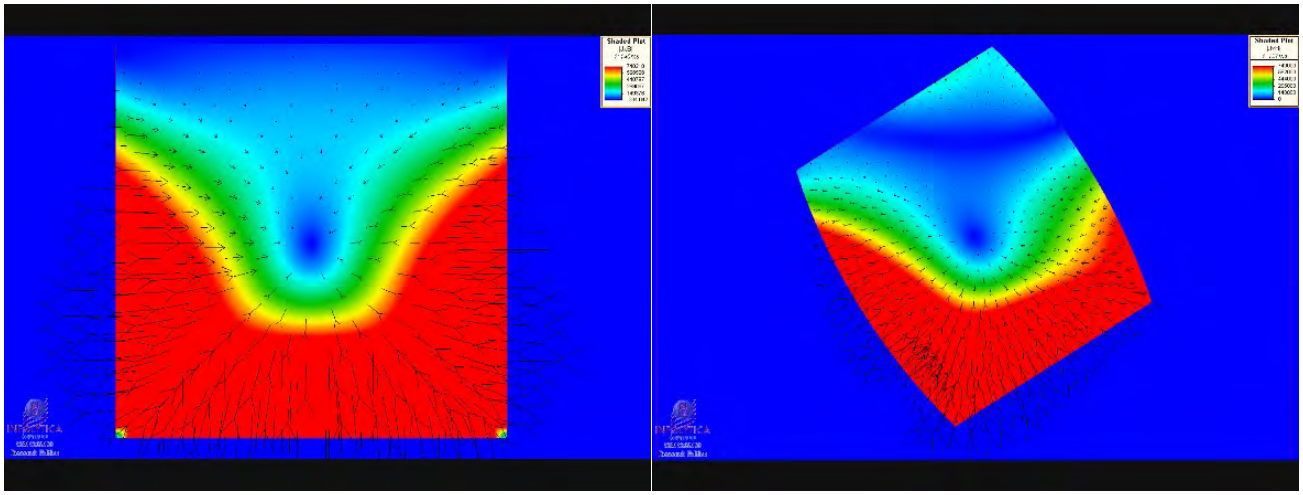

Figure 20: As the cylinder travels through the gradient, the color and arrows indicate the strength (red = strongest) and direction of the force on the cylinder. The orientation of the cylinder on the left is initially symmetric and will not rotate. The orientation of the cylinder on the right is initially offset from the normal axis. This asymmetry will cause the cylinder to be unstable and therefore rotate.

Figure 21 shows a cylinder moving in a uniform magnetic field that is parallel to the direction of the motion. It has been proposed in the literature[3] that the cylinder will decelerate to the point of stopping. This has been shown both analytically and through the software to be incorrect. In the absence of conductive losses, the deceleration pressure felt on the leading surface of the cylinder is just offset by the accelerating pressure on the trailing face of the cylinder. The energy taken to compress the magnetic field into the small space around the edge of the cylinder is given back when the field re-expands into the volume.

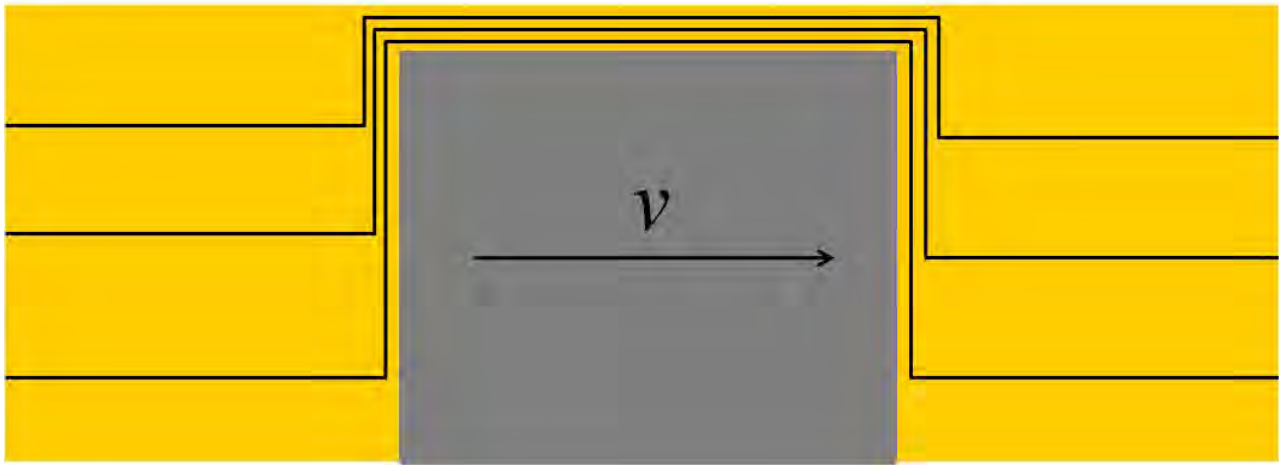

Figure 21: Above is a drawing of a cylinder moving in a uniform magnetic field that is parallel to the direction of the motion. The result is no compression or braking of the cylinder due to the absence of conductive losses.

Figure 22 shows a copper shell spinning at a rate of 8000 RPMs in a 1 Tesla uniform external field. This shell has an inner radius of 1 cm and outside 2 cm. As the cylinder rotates, the field is expelled from the center which is effectively shielded from the outside field. The color indicates the magnetic field intensity where blue is zero and red is 1 Tesla. The black lines are the field lines. Notice that these lines twist around the cylinder. The variables that affect the amount of shielding can be summed up in a dimensionless number, the (angular) magnetic Reynolds number, $R_m = \mu \sigma \Omega r^2$ where μ is the permiability, σ is the conductivity, Ω is the angular velocity and r is the radius. Therefore as the radius of the shell gets larger, the cylinder does not need to spin as rapidly. For example, this same effect would be found in a 1 meter cylinder traveling at 3.2 RPMs. This could be useful to shield vital sensitive equipment from magnetic effects.

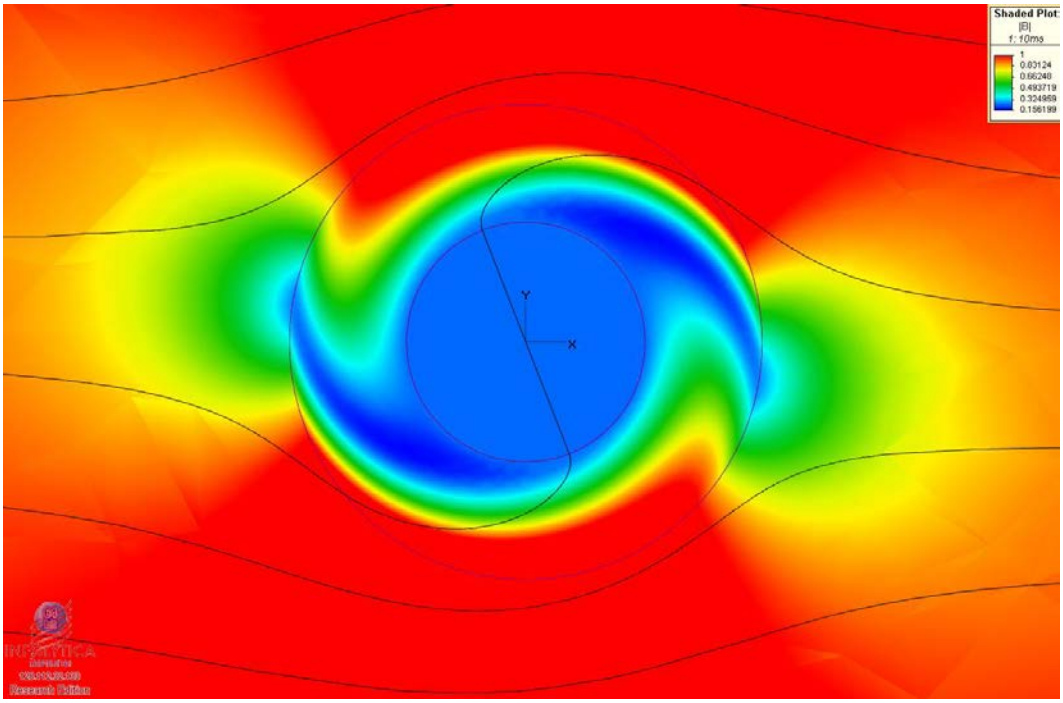

Figure 22: Above is a copper shell spinning at a rate of 8000 RPMs shielding the inside from a 1 Tesla uniform external field. This shell has an inner radius of 1 cm and outside 2 cm. The color indicates the magnetic field intensity where blue is zero and red is 1 Tesla. The black lines are the field lines.

Area 9) Future directions

Using Bayesian inference, a simplified solution was found to approximate the true magnetic field due to the Helmholtz coils. It has not yet been implemented to determine an analytical approximation for the magnetic field inside the sphere. If this was done, the stress tensor could be solved for this case. This would give an analytical approximation for the high velocity case that is very close to simulation.

It is suggested that software be found or developed for deformable models to include both the high velocity spherical case and the magnetic flux compression in 3-D. Experimental work to confirm the simulations would also be desirable.

Summary of progress:

- Completion of solid sphere experiments providing measured results for analytic and computational model validation.
- Development of analytic model of sphere fall and for flat plate fall geometries
- Evaluation and acquisition of 3-D commercial code for dynamic modeling of the interaction of materials with magnetic fields.
- Preliminary tests of 3-D commercial code for 1-D/2-D multi-layer flat plate configurations incorporating copper covered plates.
- Implementation of 3-D commercial code for low and high velocity cases.
- Evaluation of results regarding velocity and energy changes; no significant change to velocity.
- Examination of forces acting on the conducting sphere; large forces on sphere.
- Empirical approximation for high velocity case.
- Observed mechanical deformation and heating effects by ALEGRA code analysis.
- MagNet code vs. ALEGRA code discussion.
- Possible application to space debris protection.
- Approximation for magnetic field from magnetic flux compression in a box configuration.
- Additional model building related to current focus.

Key References

1. A. Paton and W. Millar, "Compression of Magnetic Field Between Two Semi-Infinite Slabs of constant Conductivity", J. Appl. Phys. 35, p1141 (1964).
2. *Protecting the Space Station from Meteoroids and Orbital Debris*, National Academy Press 1997 http://www.nap.edu/catalog/5532.html
3. J. Bennett, T. Gora, P. J. Kemmey and W. J. Kolkert, “Electromagnetic Braking of a Metallic Projectile in Flight”, *IEEE Transactions on Magnetics*, **3**, 1250-1253, 1985

Personnel supported: Dr. Adom Giffin, Postdoctoral Fellow

Subcontract to University of Minnesota, Dr. Graham Candler